Mesoporous TiO_2/SiO_2 composite nanofibers with selective photocatalytic properties†

Sihui Zhan, Dairong Chen,* Xiuling Jiao* and Yang Song

Received (in Cambridge, UK) 2nd January 2007, Accepted 31st January 2007
First published as an Advance Article on the web 21st February 2007
DOI: 10.1039/b618905a

Mesoporous TiO_2/SiO_2 composite nanofibers with a diameter of 100–200 nm and silica shell thickness of 5–50 nm have been fabricated by a sol–gel combined two-capillary co-electrospinning method; the composite nanofibers exhibited selective photocatalytic activity based on the decomposition of Methylene Blue, Active Yellow and Disperse Red.

Titania (TiO_2) is biologically and chemically inert, relatively inexpensive, and has been extensively investigated for its photocatalytic activity and applications in fields such as air cleaning, water purification and organic synthesis.[1] Many organics can be degraded to CO_2 and H_2O over TiO_2 particles and films by ultraviolet (UV) irradiation,[2] however, the application of selective photocatalysis is of particular interest because it might open new potential fields of applications such as separation processes, selective elimination or oxidation of (pollutant) molecules from a mixture where nonselective TiO_2 catalysts cannot be used.[3]

Photochemical oxidation is believed to occur when the species to be oxidized adsorb on the TiO_2 particles surface, thus the photochemical reactions at particle/solution interfaces are controlled by both relative redox energies and adsorption characteristics. To modify the selective photocatalysis on TiO_2 particles, methods including (1) surface modification with functional groups or altering the surface charge, and (2) doping with diverse transition metals such as Fe, Zn and Zr or depositing noble metals such as Ag and Pd on the particle surfaces have been developed.[4] In 2001, Calza *et al*. found that size-selective photo-catalytic activity was promoted by catalytic systems based on zeolitic materials containing Ti chains, which allowed a preferential conversion of either small or large molecules.[5] Since then, porous photocatalysts have attracted much attention because of their advantages such as: (1) high surface-to-volume ratio, which allows increased adsorption of various reactants and products during the photocatalytic reaction, (2) uniform pore-size distribution, which is of great importance in selective adsorption of organic molecules, and (3) high catalytic activity, which is favorable to completely degrade the organic molecules to CO_2 and H_2O.[6] However, particulate catalysts might re-pollute treated water because of the tremendous difficulties in recovery. However, using supporting substrates such as glass beads/fibers, zeolite, active carbon, *etc.*, particle catalysts leads to lower catalytic efficiency.[1,2] Compared with the corresponding particles, electrospun TiO_2 based fibers,[7] especially mesoporous TiO_2 fibers are considered good candidates because of their high photocatalytic activity and ease of removal, but they are brittle and lack selectivity in the oxidative decomposition of organic molecules.[8] Therefore, the development of a novel photo-catalyst with selectivity, high activity and favorable recycling characteristics is a challenge for practical applications.

In this communication, mesoporous TiO_2/SiO_2 composite nanofibers fabricated by use of a combined sol–gel and two-capillary co-electrospinning[9] method to modify the selectivity of the TiO_2 photocatalyst are introduced. In addition, the amorphous silica coating on the mesoporous TiO_2 nanofibers' surface enhances their strength and is favorable for applications.

The spinnable silicic sol (see ESI†) was poured into the outer tube, and the titanic sol prepared as in our previous report was placed in the inner capillary.[8] The two fluids were pressurized with N_2 to drive them to the spinneret tip which was connected to a high-voltage supply (BGG-200 kV/20 mA). As the pressures of the inner and outer tubes increased, the titanic and silicic sols were simultaneously ejected to form composite gel nanofibers. During the electrospinning process, the applied voltage was 25 kV, the distance between spinneret and collector was 25 cm, and the temperature was maintained at 22.0 °C. Finally, the produced xerogel nanofibers were collected, dried at room temperature for 24.0 h, then heated at 130 °C for 8.0 h and calcined at 400 °C for 4.0 h to completely eliminate the organics (based on TG and IR results, see ESI, Fig. S1†).

The rheological curves of these two precursor sols show that they are Newtonian fluids. The pH, composition and rheological properties of the sols have important effects on the formation of mesostructured materials.[8] In the present work, the pH value and composition of the precursor sols are kept as described above. By varying the viscosity of the sol with the aging time, the optimal sol viscosity (RS75 rheometer, HAAKE Co.) for the fabrication of mesostructured nanofibers was determined to be 5 Pa s, although the viscosity range suitable for the formation of electrospun nanofibers is 1–9 Pa s.

The scanning electron microscope (FE-SEM, JSM-6700F) image (Fig. 1(a)) shows that the composite xerogel nanofibers with uniform diameter of *ca*. 100–200 nm exhibit smooth surfaces. After calcination, the nanofibers still retain their original morphology without cracking (Fig. 1(b)), but they shrink slightly with the removal of organics. The titanic and silicic precursor sols are miscible, so it is difficult to distinguish the interface of the composite xerogel nanofibers from the SEM images. However, when the sintered nanofibers are ground into powders,

School of Chemistry and Chemical Engineering, Shandong University, Jinan, 250100, People's Republic of China. E-mail: cdr@sdu.edu.cn; Fax: +86-531-88364281; Tel: +86-531-88364280

† Electronic supplementary information (ESI) available: Experimental details, TG curves, FTIR spectra, HR-TEM micrograph and UV-vis spectra. See DOI: 10.1039/b618905a

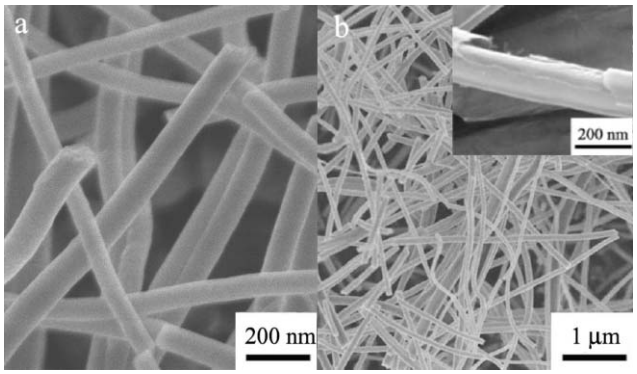

Fig. 1 SEM images of (a) xerogel nanofibers, (b) composite nanofibers.

the core/shell structure of nanofibers can be seen from the crashed shells in the SEM image (inset of Fig. 1(b)).

The LA-XRD (Rigaku D/Max 2200PC, Cu-Kα radiation, λ = 0.15418 nm) pattern of the xerogel nanofibers (see ESI, Fig. S2†) shows two peaks centered at 2θ = 0.85 and 1.70°, corresponding to a *d*-spacing of 10 and 5 nm, which indicates the nanofibers are mesostructured. Taking into account the orientation of the fibers in sampling during XRD analysis, the LA-XRD pattern was recorded after the nanofibers were ground into powders to avoid orientation. As a result, the LA-XRD pattern exhibited three reflections at 2θ = 0.85, 1.47, 1.70, which were indexed to (100), (110) and (200) reflections of the hexagonal structured material,[8] indicating the hexagonal mesostructure of the composite nanofibers. After calcination at 400 °C in air, the first peak shifts to 2θ = 1.2° corresponding to a *d*-value of 7.3 nm with decreased intensity and broadening, indicating that the order and basal *d*-spacing of the mesostructures has decreased. This might be due to the shrinkage of both the mesopores and the framework during the removal of organics and crystallization of anatase TiO_2. The XRD pattern shows that anatase TiO_2 is formed after calcination at 400 °C in air, and the mean size of anatase TiO_2 nanocrystals is *ca.* 7 nm as calculated by the Scherrer equation, which is consistent with the HR-TEM result. The well-resolved XRD peaks indicate the highly crystalline nature of the mesoporous framework.[10] The XRD pattern shows no obvious amorphous SiO_2 peak because of the small quantity of silica shells.

The high-resolution TEM (HR-TEM, GEOL-2010) images (Fig. 2) show the mesoporous channel architecture and hierarchical structure of one typical nanofiber. The TiO_2 core exhibits

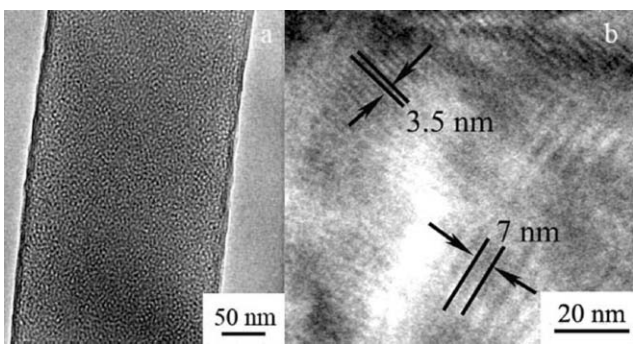

Fig. 2 HR-TEM images of TiO_2/SiO_2 composite nanofibers (a) and the fiber ends after they were microtomed into thin slices (b).

mesoporous channels from 6 to 8 nm, which is in agreement with the low-angle XRD patterns.[8] As shown in Fig. 2(b), there are two different sizes of mesoporous channel at the end of a single composite fiber. One is the 3.5 nm distance between two immediate channels, which belongs to the mesoporous SiO_2 shell, the other is a 7.0 nm distance, which is attributed to the mesoporous TiO_2 core (see ESI, Fig. S3(a)†).

N_2 adsorption–desorption isotherms (Quantachrom SI) and calculated pore size distribution curves based on the density functional theory (DFT) method of the composite nanofibers and the nanofibers after dissolving away the SiO_2 shell or the TiO_2 core are shown in Fig. 3. The BET surface area and specific pore volume of the composite nanofibers are 353.7 $m^2\ g^{-1}$ and 0.33 $cm^3\ g^{-1}$, respectively. The adsorption–desorption isotherms of the TiO_2 core (curve 1) and SiO_2 shell (curve 3) are different, and that of the core/shell nanofibers (curve 2) is made up of these two different mesopores. After dissolving the SiO_2 shell with HF, mesoporous TiO_2 nanofibers with pore size of 6–8 nm are obtained (see ESI, Fig. S3(b)†). However, when the TiO_2 core is dissolved away with sulfuric acid, the SiO_2 shell is too thin to retain the hollow nanofiber morphology and the product is thin mesoporous silica layers with pore sizes ranging from 3 to 4 nm (see ESI, Fig. S3(c); EDS, Fig. S4†). For the core/shell nanofibers (curve 2), two hysteresis loops appear in the relative pressure (P/P_0) ranges of 0.41–0.50 and 0.65–1.0, which are attributed to the primary pores of the mesoporous SiO_2 shell and the TiO_2 core, respectively. In the relative pressure (P/P_0) range of 0.41–0.50, the area of the H1 hysteresis loop is very small, and adsorption and desorption curves are almost superimposed, indicating relatively small pores in the shell compared to those in the TiO_2 core. There is another typical H1 hysteresis loop with a sharp increase of the adsorbed volume at P/P_0 = 0.65, indicating the presence of well-developed mesopores in the TiO_2 cores.

Below a relative pressure of 0.05, the adsorption increases sharply at low pressures (curves 2 and 3 in Fig. 3), indicating a nanoporosity in the silica shells. For the same sample, the DFT approach used to determine the mesopore size has fundamental advantages over the classical BJH method.[11] Here, using the DFT method, we found that two different pore size distributions exist in the mesoporous SiO_2 shell, 1.3 nm and 4.2 nm (curve 3 in ESI, Fig. S5(b)†), which is in accordance with the size of 4 nm

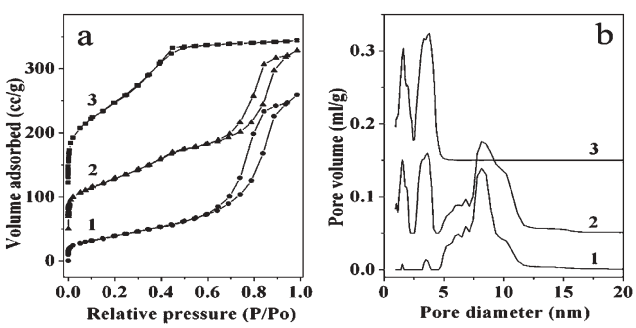

Fig. 3 N_2 adsorption–desorption isotherms (a) and the pore size distribution curves based on the DFT method (b) of nanofibers after dissolving SiO_2 (1), the composite nanofibers (2), and SiO_2 shells after dissolving TiO_2 (3). The adsorption isotherms for samples 2 and 3 are shifted by 50 and 100 $cm^3\ g^{-1}$, while the pore volumes are shifted by 0.05 and 0.10 mL g^{-1}, respectively.

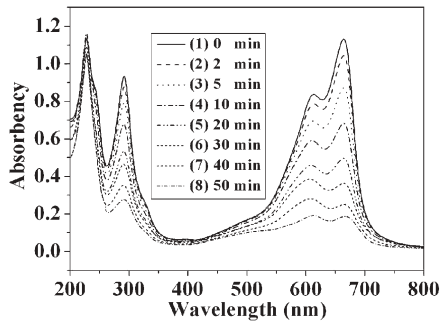

Fig. 4 UV-visible spectra of MB and DR mixed solution under UV photocatalysis in the presence of the composite nanofibers.

calculated based on BJH theory from the desorption branch of the isotherm and observed in the HR-TEM images (Fig. 2). The existence of additional nanopores in the composite nanofibers may be due to the strong interlinkage of hydrophilic EO blocks with silica species during solidification at the initial stage of gel formation. After calcination, the micelles decompose and the microstructures shrink to form a large number of nanopores.[12]

The selective photocatalytic activities (see ESI, Experimental section†) of the composite nanofibers were investigated by photo-oxidation of Methylene Blue (MB) and Disperse Red S-3GFL dyes (DR).[13] The absorptions at 664 and 228 nm are proportional to the concentrations of MB and DR, respectively and the concentrations of these two dyes are measured as a function of irradiation time. Using the nanofibrous cores after dissolution of SiO_2 as photo-catalyst, the absorptions of both MB and DR almost completely disappear after irradiation for 50 min (see ESI, Fig. S5†). However, using the composite nanofibers as the photocatalyst, only the absorption peaks of MB disappear and the DR absorption at 228 nm hardly changes (Fig. 4).[14]

Further experiments indicate that in the absence of catalyst DR and MB hardly decompose under UV light irradiation. (see ESI, Fig. S6†) While in the presence of the composite nanofibers, the photo-degradation rate of MB is faster than that by P25, so the composite nanofibers had good photocatalytic activity for the decomposition of MB (see ESI, Fig. S6(b)†) Disperse red S-3GFL is comprised of nonionic organic compounds which have low solubility in water, so they form aggregates which are much bigger than the mesoporous channels in the SiO_2 shells. This hypothesis is supported by filtration and dialysis experiments (see ESI, Fig. S7†). Since the catalytic centers are located in the TiO_2 core, it can be concluded that the internal channels of mesoporous silica protect against entrance of large species such as DR. However, MB molecules can easily cross the channels to be decomposed on the TiO_2 surface because of their small size. Size seems to be the main factor in determining the selective degradation which can be thought of as "pore-mouth" selectivity.[5] Because MB absorbs in the visible region, which is different from the DR, active yellow K-4G (AY) with only UV absorption was also selected to test the selective photo-catalytic activity.[15] As a result, the mesoporous composite nanofibers also exhibit excellent photo-catalytic activity on the decomposition of AY (see ESI, Fig. S8†).

This work was supported by Program for New Century Excellent Talents in University, P. R. China. The authors thank Dr Pamela Holt for editing the manuscript.

Notes and references

1 (*a*) M. R. Hoffmann, S. T. Martin, W. Choi and D. W. Bahnemann, *Chem. Rev.*, 1995, **95**, 69; (*b*) O. Carp, C. L. Huisman and A. Reller, *Prog. Solid State Chem.*, 2004, **32**, 33; (*c*) G. J. de A. A. Soler-Illia, C. Sanchez, B. Lebeau and J. Patarin, *Chem. Rev.*, 2002, **102**, 4093; (*d*) H. Shibata, T. Ogura, T. Mukai, T. Ohkubo, H. Sakai and M. Abe, *J. Am. Chem. Soc.*, 2005, **127**, 16396.
2 (*a*) D. M. Antonelli, *Microporous Mesoporous Mater.*, 1999, **30**, 315; (*b*) H. S. Yun, K. Miyazawa, H. Zhou, I. Honma and M. Kuwabara, *Adv. Mater.*, 2001, **13**, 1377; (*c*) Z. Y. Yuan, T. Z. Ren and B. L. Su, *Adv. Mater.*, 2003, **15**, 1462; (*d*) H. Luo, C. Wang and Y. Yan, *Chem. Mater.*, 2003, **15**, 3841.
3 P. Du, J. A. Moulijn and G. Mul, *J. Catal.*, 2006, **238**, 342.
4 (*a*) T. Ohno, T. Tsubota, K. Kakiuchi, S. Miyayama and K. Sayama, *J. Mol. Catal. A: Chem.*, 2006, **245**, 47; (*b*) G. Palmisano, M. Addamo, V. Augugliaro, T. Caronna, E. García-López, V. Loddo and L. Palmisano, *Chem. Commun.*, 2006, 1012; (*c*) J. C. Colmenares, M. A. Aramendía, A. Marinas, J. M. Marinas and F. J. Urbano, *Appl. Catal. A: Gen.*, 2006, **306**, 120; (*d*) X. M. Yang, D. A. Tryk, K. Hashimoto and A. Fujishima, *J. Phys. Chem. B*, 1998, **102**, 4933.
5 P. Calza, C. Pazè, E. Pelizzetti and A. Zecchina, *Chem. Commun.*, 2001, 2130.
6 (*a*) Y. Shiraishi, N. Saito and T. Hirai, *J. Am. Chem. Soc.*, 2005, **127**, 8304; (*b*) J. Li, W. Ma, Y. Huang, M. Cheng, J. Zhao and J. C. Yu, *Chem. Commun.*, 2003, 2214; (*c*) F. X. Llabrés i Xamena, P. Calza, C. Lamberti, C. Prestipino, A. Damin, S. Bordiga, E. Pelizzetti and A. Zecchina, *J. Am. Chem. Soc.*, 2003, **125**, 2264.
7 (*a*) M. Macias, A. Chacko, J. P. Ferraris and K. J. Balkus, Jr., *Microporous Mesoporous Mater.*, 2005, **86**, 1; (*b*) D. Li, J. T. McCann and Y. Xia, *Small*, 2005, **1**, 83; (*c*) Y. Xia and D. Li, *US Pat. Appl.*, 2006, 8 pp.; (*d*) M. Jin, X. Zhang, S. Nishimoto, Z. Liu, D. A. Tryk, A. V. Emeline, T. Murakami and A. Fujishima, *J. Phys. Chem. C*, 2007, **111**, 658; (*e*) R. Ostermann, D. Li, Y. Yin, J. T. McCann and Y. Xia, *Nano Lett.*, 2006, **6**, 1297.
8 S. Zhan, D. Chen, X. Jiao and C. Tao, *J. Phys. Chem. B*, 2006, **110**, 11199.
9 (*a*) D. Li and Y. Xia, *Nano Lett.*, 2003, **3**, 555; (*b*) J. Doshi and D. H. Reneker, *J. Electrostatics*, 1995, **35**, 151; (*c*) I. G. Loscertales, A. Barero, I. Guerrero, R. Cortijo, M. Marquez and A. M. Ganan-Calvo, *Science*, 2002, **295**, 1695; (*d*) R. Dersch, M. Steinhart, U. Boudriot, A. Greiner and J. H. Wendorff, *Polym. Adv. Technol.*, 2005, **16**, 276; (*e*) Z. Liu, D. D. Sun, P. Guo and J. O. Leckie, *Nano Lett.*, 2006, DOI: 10.1021/nl061898e; (*f*) M. Jin, X. Zhang, A. V. Emeline, Z. Liu, D. A. Tryk, T. Murakami and A. Fujishima, *Chem. Commun.*, 2006, 4483.
10 (*a*) C. J. Brinker, Y. Lu, A. Sellinger and H. Fan, *Adv. Mater.*, 1999, **11**, 579; (*b*) D. Grosso, G. J. de A. A. Soler-Illia, F. Babonneau, C. Sanchez, P. Albouy, A. Brunet-Bruneau and A. R. Balkenende, *Adv. Mater.*, 2001, **13**, 1085.
11 (*a*) B. Smarsly, S. Polarz and M. Antonietti, *J. Phys. Chem. B*, 2001, **10**, 10473; (*b*) A. V. Neimark and P. I. Ravikovitch, *Langmuir*, 1997, **13**, 5148; (*c*) M. Jaroniec and L. A. Solovyov, *Langmuir*, 2006, **22**, 6757.
12 (*a*) P. Yang, D. Zhao, B. F. Chmelka and G. D. Stucky, *Chem. Mater.*, 1998, **10**, 2033; (*b*) M. Kruk, M. Jaroniec, C. H. Ko and R. Ryoo, *Chem. Mater.*, 2000, **12**, 1961; (*c*) V. Zelenak, V. Hornebecq, S. Mornet, O. Schaf and P. Llewellyn, *Chem. Mater.*, 2006, **18**, 3184.
13 (*a*) S. Lee, M. Sheridan and A. Mills, *Chem. Mater.*, 2005, **17**, 2744; (*b*) E. Stathatos, T. Petrova and P. Lianos, *Langmuir*, 2001, **17**, 5025.
14 (*a*) T. W. Chung, B. J. Kim, S. Y. Park, T. Akaike, J. W. Nah and C. S. Cho, *Macromolecules*, 2000, **33**, 8921; (*b*) J. C. Yu, L. Zhang and J. Yu, *Chem. Mater.*, 2002, **14**, 4647; (*c*) Y. Zhu, L. Zhang, L. Wang, Y. Fu and L. Cao, *J. Mater. Chem.*, 2001, **11**, 1864.
15 X. Yan, T. Ohno, K. Nishijima, R. Abe and B. Ohtani, *Chem. Phys. Lett.*, 2006, **429**, 606.